Supplementary Information for:

Controlling the molecular arrangement of racemates through weak interactions: the synergy between π-interactions and halogen bonds

Carlos Romero-Nieto,[a,b] A. de Cózar,*[c,d] Elzbieta Regulska,[a,b] John B. Mullenix,[a] Frank Rominger,[a] Philip Hindenberg[a]*

[a] Organisch-Chemisches Institut, Ruprecht-Karls-Universität Heidelberg, Im Neuenheimer Feld 270, 69120 Heidelberg, Germany. E-mail: carlos.romero.nieto@oci.uni-heidelberg.de

[b] Faculty of Pharmacy, University of Castilla-La Mancha, Calle Almansa 14 - Edif. Bioincubadora, 02008, Albacete, Spain

[c] Departamento de Química Orgánica I, Facultad de Química, Universidad del País Vasco P. K. 1072, E-20018, San Sebastián-Donostia, Spain. E-mail: abel.decozar@ehu.eus

[d] IKERBASQUE, Basque Foundation for Science, Bilbao, Spain

Table of Contents:

1. General section:

Reactions were carried out in dry glassware and under inert atmosphere of purified argon or nitrogen using Schlenk techniques. CH_2Cl_2 and THF were used directly from a solvent purification system MB SPS-800. Dried deuterated solvents were dried over molecular sieves. 2-bromo-3-(4,4,5,5-tetramethyl-1,3,2-dioxaborolan-2-yl)pyridine and 1,2,4,5-tetrafluoro-3,6-diiodobenzene were prepared according to protocols described by others.[S1a,b] Compounds **1** and **2**, 3-(8-bromonaphthalen-1-yl)pyridine and 4-(8-bromonaphthalen-1-yl)pyridine were synthesized according to our previously reported protocols.[S1c]

NMR: ^{1}H, ^{13}C, and ^{31}P NMR as well as COSY spectra were recorded on a Bruker Avance III, Bruker Avance 400, Bruker Avance-III-300, Bruker Avance DRX-300, Bruker Avance 500 or Bruker Avance 600. Chemical shifts are expressed as parts per million (ppm, δ) and referenced to external 85% H_3PO_4 (^{31}P), or solvent signals (^{1}H / ^{13}C): $CDCl_3$ (7.27 / 77.16 ppm) as internal standards. Signal descriptions include: s = singlet, d = doublet, t = triplet, q = quartet, m = multiplet and br = broad. All coupling constants are absolute values and *J* values are expressed in Hertz (Hz).

Mass spectrometry: MS and HRMS were measured at the Institute of Organic Chemistry of the University of Heidelberg. A Bruker ApexQe FT-ICR was used for ESI spectra and a JEOL JMS-700 MS for EI^{+}. GCMS was performed with a GC system 7890a from Agilent Technologies.

X-Ray crystallography: X-ray crystal structure analyses were measured on Bruker Smart CCD or Bruker Smart APEX instrument using Mo-Kα radiation. Diffraction intensities were corrected for Lorentz and polarization effects. An empirical absorption correction was applied using SADABS[S2] based on the Laue symmetry of reciprocal space. Heavy atom diffractions were solved by direct methods and refined against F2 with the full matrix least square algorithm. Hydrogen atoms were either isotropically refined or calculated. The structures were solved and refined using the SHELXTL[S3] software package. The crystal structure of **1** (CCDC 2023735) was obtained by crystallization from DCM, crystals of **adduct 1** (CCDC 2023736) and **adduct 2** (CCDC 2023737) were grown by slow diffusion of *n*-pentane into a saturated solution of DCM, the crystal structure of **2** (CCDC 1418421) was obtained according to a previously reported method.[S1c]

Attempts for the co-crystallization of 2	**Results**
Slow concentration from MeOH	Unsuccessful
Slow concentration from chloroform	Unsuccessful
Slow concentration from dichloromethane	Unsuccessful
Vapor diffusion of pentane into dichloromethane	Unsuccessful
Liquid diffusion of MeOH into dichloromethane	Unsuccessful
Liquid diffusion of MeOH into chloroform	Unsuccessful
Liquid diffusion of pentane into dichloromethane	Successful

Theoretical calculations: All DFT calculations were carried out by using the Amsterdam Density Functional (ADF) program.[S4] TZ2P basis set which is of triple-ζ quality and has been augmented with two polarization function sets: 2p and 3d on hydrogen, 3d and 4f on fluorine and iodine atoms.
Energies were calculated at the wB97X-D[S5] level of the generalized gradient approximation (GGA).[S6] This range–separated hybrid functional that includes non-local correlation (W10) and dispersion corrections (by means of Grimme's D3 BJDAMP model)[S7] has been shown to be of adequate accuracy for the treatment of similar compounds showing halogen bonding interactions (X-bond).[S8] Relativistic effects were accounted for by using the zero[th]-order regular approximation (ZORA).[S9]
Intermolecular interactions were computed by using the fragment analysis feature included on ADF suite of programs. With this method the wavefunction of the complete system is compared to the sum of the wavefunctions of the fragments and the difference is analyzed within the Kohn-Sham MO conceptual framework according to the Energy Decomposition Analysis (EDA)[S10] as

$$\Delta E_{\text{int}}(\zeta) = \Delta V_{\text{elstat}}(\zeta) + \Delta E_{\text{Pauli}}(\zeta) + \Delta E_{\text{oi}}(\zeta) + \Delta E_{\text{disp}}(\zeta) \quad (1)$$

Herein, $\Delta V_{\text{elstat}}(\zeta)$ is the classical Coulombic interaction between the unperturbed charge distribution of each of the two fragments. The term $\Delta E_{\text{Pauli}}(\zeta)$ describes the Pauli repulsions between occupied orbitals of the two fragments and is responsible for steric repulsion. The term $\Delta E_{\text{oi}}(\zeta)$ stands for the stabilizing orbital interaction energy, including charge transfer (such as HOMO–LUMO interactions). Finally, $\Delta E_{\text{disp}}(\zeta)$ corresponds to the dispersion interactions.

The electron density distribution is analyzed using the Voronoi deformation density (VDD) method for computing atomic charges.[S11] The VDD atomic charge (Q_A) is computed as the numerical integral of the deformation density in the volume of the Voronoi cell of atom A, that is, the compartment of space bounded by the bond midplanes on and perpendicular to all bond axes between nucleus A and its neighboring nuclei (Eq. 2).

$$Q_A = \int [\rho(r) - \sum_B \rho_B(r)]\, dr \quad (2)$$

Here, $\rho(r)$ is the electronic density of the molecule and $\sum_B \rho_B(r)$ is the superposition of atomic densities $\rho_B(r)$ of a fictitious promolecule without chemical interactions where all atoms are considered neutral. Therefore, Q_A directly measures the charge that flows out of ($Q_A > 0$) or into ($Q_A < 0$) the Voronoi cell of atom A due to chemical interactions, and not the charge value of the atom A.

Electrostatic surface potentials (PES) mapped on the 0.001 a.u. electron isodensity and the estimated maximum and minimal values ($V_{s,max}$ and $V_{s,min}$ respectively) as well as at selected points were computed with the ADFview program.

Steady-state spectroscopy: Absorption and emission spectra were recorded from DCM solutions using a Jasco V660 and Jasco FP6500 spectrometer, respectively.

Fluorescence quantum yields Φ: Quantum yields in solution were calculated relative to quinine sulfate in 0.1 M sulfuric acid as a reference (Φ = 0.54 according to the literature[S12]) from five dilutions and using the formula:

$\Phi_x = \Phi_{st} (Grad_x/Grad_{st}) (n_x^2/n_{st}^2)$

Φ_x: quantum yield of sample X

Φ_{st}: quantum yield of the reference

$Grad_x$: Gradient from the plot of integrated fluorescence intensity vs absorbance of the sample x

$Grad_{st}$: Gradient from the plot of integrated fluorescence intensity vs absorbance of the reference

n_x: refractive index from the solvent employed with the sample X

n_{st}: refractive index from the solvent employed with the reference

Quantum yields in the solid state were measured with a calibrated Ulbricht sphere; values are an average from at least two independent measurements.

Fluorescence lifetimes τ: The fluorescence decays were recorded with a HORIBA Scientific Fluorocube single photon counting system operated with HORIBA Scientific DataStation version 2.2. Fluorescence lifetimes were acquired by an exponential fit according to the least mean square with commercially available software HORIBA Scientific Decay Data Analyses 6 (DAS6) version 6.4.4.

Deactivation pathways constants: Radiative decay constant (k_r) was calculated according to the following equation: $k_r = \Phi / \tau$; while the non-radiative decay constant (k_{nr}) was calculated using the following formula: $k_{nr} = (1–\Phi) / \tau$.

2. Experimental Details

2.1. Synthetic procedures

(Compound 1) 7-phenylbenzo[4,5]phosphinolino[2,3-b]pyridine 7-oxide

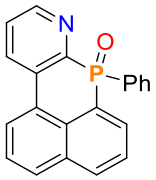

The synthesis was performed by following our previously reported protocol.[S1c] The product was obtained by washing with pentane and then ethyl acetate (Yield: 51%). **^{1}H NMR** (600 MHz, $CDCl_3$) δ 8.83 (d, *J* = 4.40 Hz, 1 H), 8.60 (t, *J* = 7.29 Hz, 1 H), 8.44 (d, *J* = 7.43 Hz, 1 H), 8.29 (dd, *J* = 14.03, *J* = 7.15 Hz, 1 H), 8.19 (d, *J* = 8.25 Hz, 1 H), 8.07 (d, *J* = 7.98 Hz, 1 H), 7.75 (t, *J* = 7.98 Hz, 1 H), 7.72 (t, *J* = 7.15 Hz, 1 H), 7.61 (dd, *J* = 12.65, *J* = 7.98 Hz, 1 H), 7.55 (dd, *J* = 8.25, *J* = 4.40 Hz, 1 H), 7.44 (t, *J* = 7.43 Hz, 1 H), 7.36 (t, *J* = 7.57 Hz, 2 H). **^{13}C{^{1}H}{^{31}P} NMR** (151 MHz, $CDCl_3$): δ 150.9, 150.7, 135.0, 134.7, 134.0, 133.6, 131.9, 131.8, 131.7, 131.5, 129.1, 128.5, 127.4, 127.2, 126.7, 126.5, 126.0, 125.4. **^{31}P{^{1}H} NMR** (243 MHz, $CDCl_3$): δ 4.69 (s, 1 P). **HRMS** (EI^+) calcd. for $C_{21}H_{14}NOP$ 327.08075, found 327.07894.

2.2. Crystallographic data

Compound 1

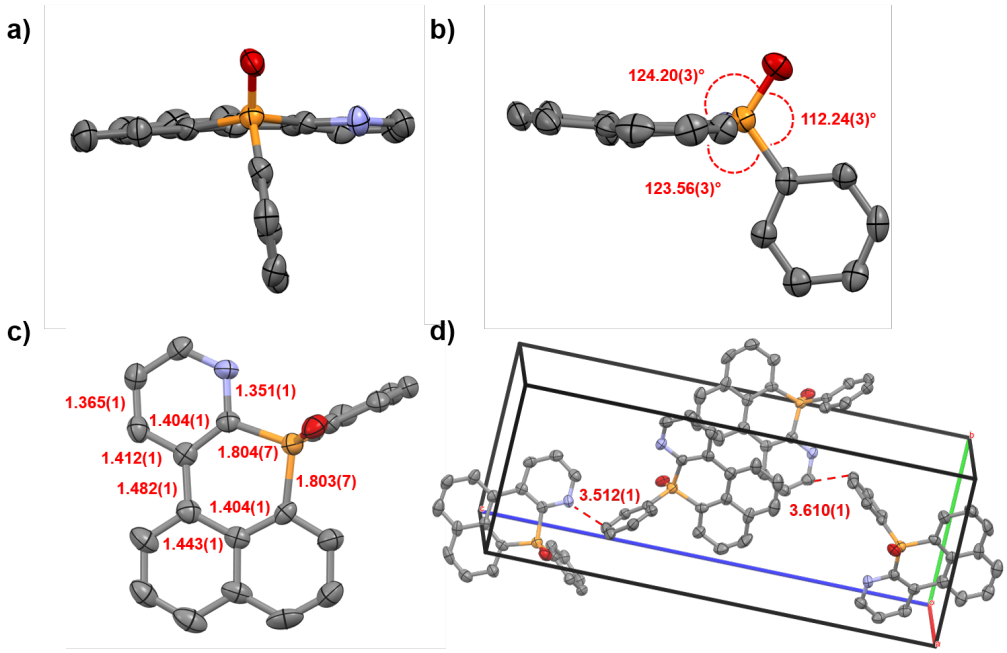

Figure S1. X-ray structures of **1** (50% probability level ellipsoids). a) front view, b) side view, c) top view, and d) crystal packing. Hydrogens have been omitted for clarity. Bond distances are in angstrom and angles in degrees.

Compound 2[S1c]

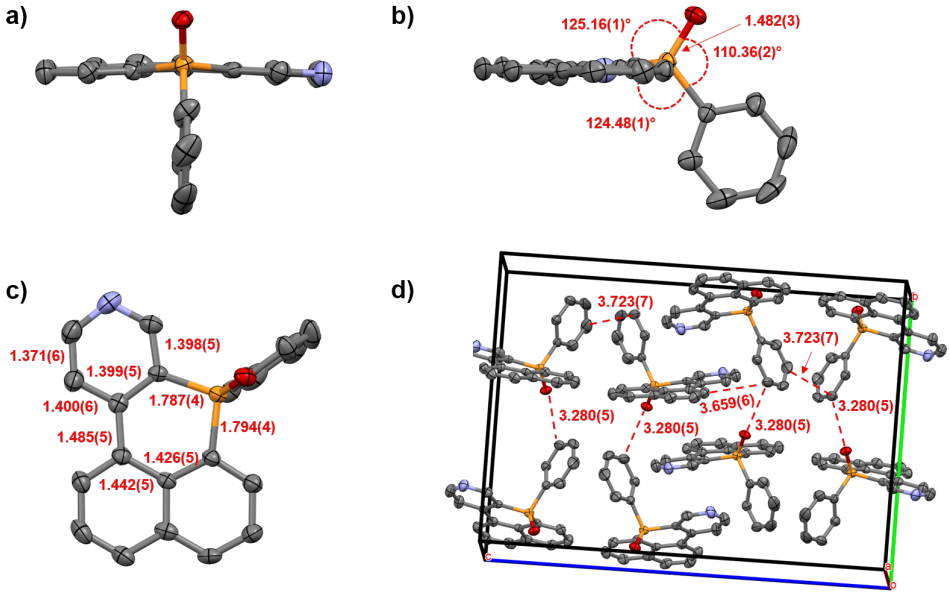

Figure S2. X-ray structures of **2** (50% probability level ellipsoids). a) front view, b) side view, c) top view, and d) crystal packing. Hydrogens have been omitted for clarity. Bond distances are in angstrom and angles in degrees.

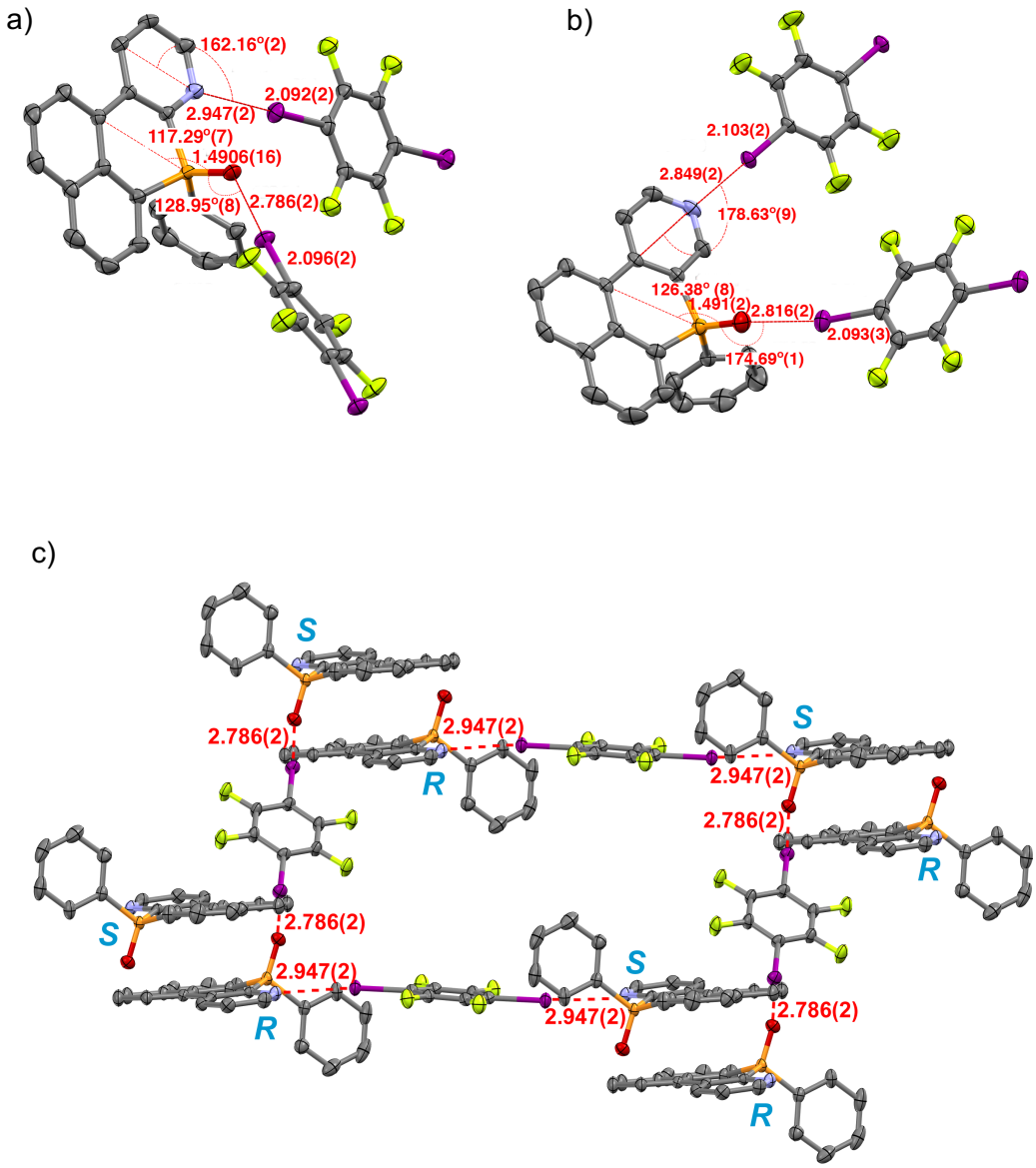

Figure S3. X-ray structures of: a) co-crystal of **1** with **A**, b) co-crystal of **2** with **A** and c) 3D assembly of co-crystal of **1** with A. (50% probability level ellipsoids). Bond distances are in angstrom and angles in degrees.

Compound 1

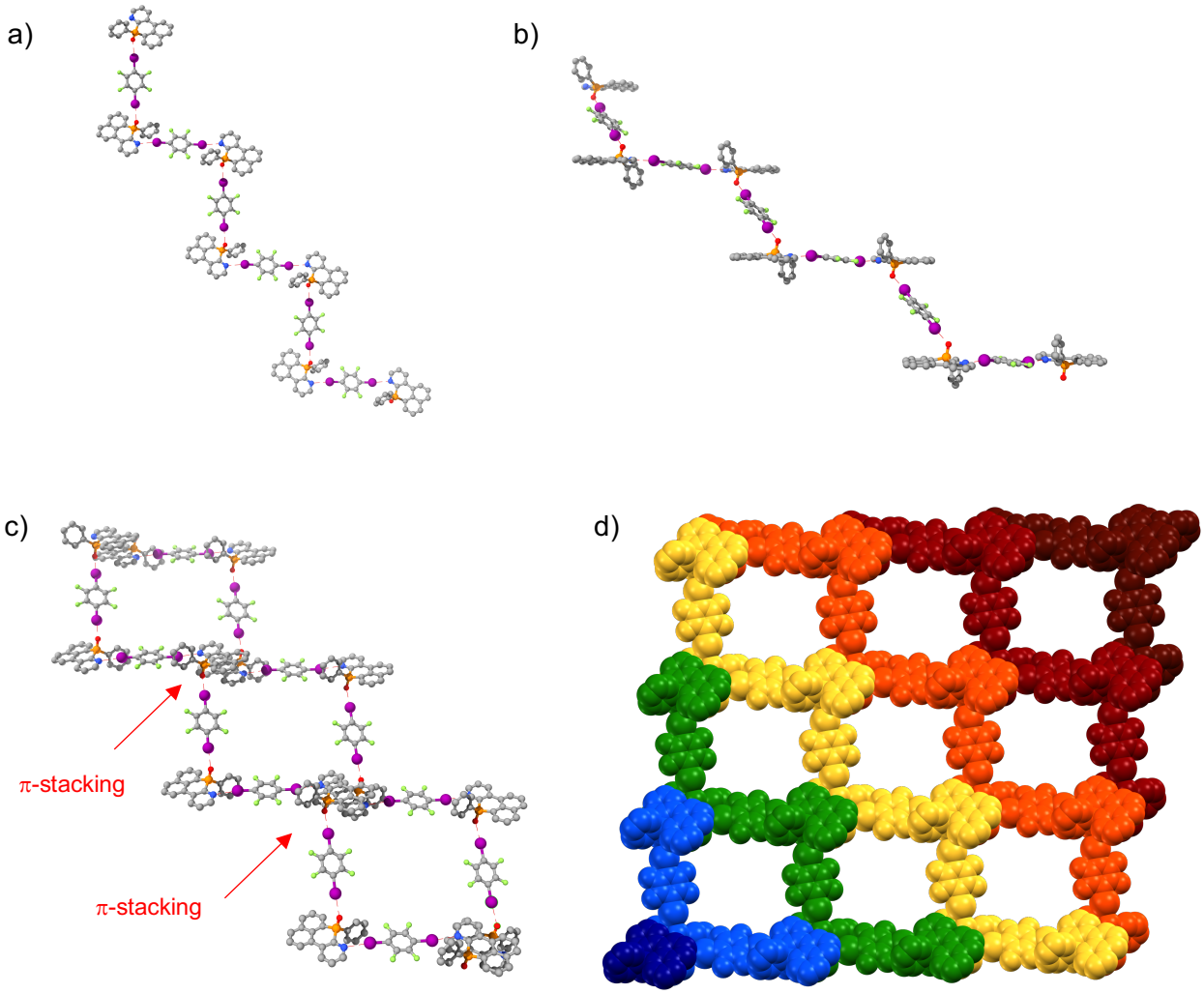

Figure S4. Zig-zag structures formed by hydrogen bonds obtained by X-ray diffraction of **adduct 1** (co-crystal of **1** with **A**): a) top view, b) front view, c) zig-zag structures bonded through π-stacking (see Table S2 for distances). d) Quadrangular structures formed by the linkage of zig-zag motifs through π-stacking. Colors indicate the zig-zag motifs.

Compound 2

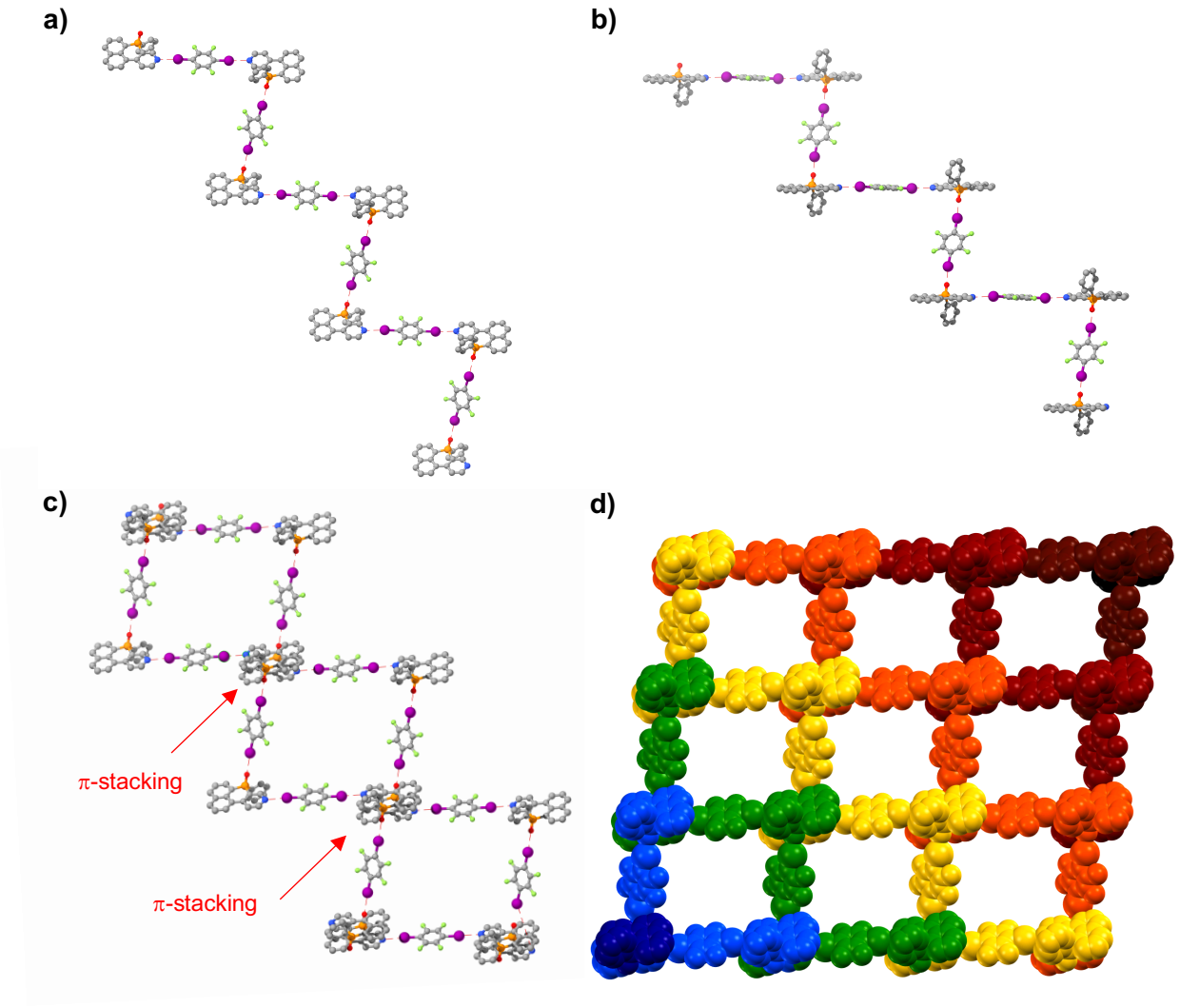

Figure S5. Zig-zag structures formed by hydrogen bonds obtained by X-ray diffraction of **adduct 2** (co-crystal of **2** with **A**): a) top view, b) front view, c) zig-zag structures bonded through π-stacking (see Table S2 for distances). d) Quadrangular structures formed by the linkage of zig-zag motifs through π-stacking. Colors indicate the zig-zag motifs.

Table S1. Selected crystallographic data of **1**, **adduct 1** and **adduct 2**.

	Compound 1	**Adduct 1**	**Adduct 2**
Empirical formula	$C_{21}H_{14}NOP$	$C_{27}H_{14}F_4I_2NOP$	$C_{30}H_{14}F_6I_3NOP$
Molecular weight	327.30	729.16	930.09
Temperature	200(2) K	200(2) K	200(2) K
Wavelength	0.71073 Å	0.71073 Å	0.71073 Å
Crystal system	orthorhombic	triclinic	triclinic
Space group	$P2_12_12_1$	P-1	P-1
Z	4	2	2
a/α	7.4610(7) Å; α = 90°	a = 10.2170(4) Å α = 85.5466(9)°	a = 8.9001(6) Å α = 99.4474(9)°
b/β	9.0095(8) Å; β = 90°	b = 10.7286(4) Å β = 72.5399(9)°	b = 13.1997(9) Å β = 97.4134(10)°
c/γ	23.283(2) Å; γ = 90°	c = 13.1032(5) Å γ = 64.1678(8)°	c = 13.3554(9) Å γ = 105.2813(9)°
Volume	1565.0(3) $Å^3$	1230.85(8) $Å^3$	1468.30(17) $Å^3$
Density (calculated)	1.389 g/cm^3	1.97 g/cm^3	2.10 g/cm^3
Absorption coefficient	0.182 mm^{-1}	2.67 mm^{-1}	3.31 mm^{-1}
Crystal shape	plate	brick	plank
Crystal size	0.060 x 0.050 x 0.040 mm^3	0.147 x 0.110 x 0.104 mm^3	0.192 x 0.142 x 0.102 mm^3
Crystal colour	colourless	colourless	colourless
Theta range for data collection	1.75 to 22.02°	1.6 to 32.4°	1.6 to 31.3°
Index Ranges	-8≤h≤8, -10≤k≤10, -27≤l≤27	-15≤h≤15, -16≤k≤16, -19≤l≤19	-12≤h≤12, -18≤k≤19, -19≤l≤19
Reflections collected	10079	57841	32986
Independent reflections	2752 (R(int) = 0.1036)	8497 (R(int) = 0.0367)	8898 (R(int) = 0.0238)
Observed reflections	1642 (l > 2σ (l))	6865 (l > 2σ (l))	7480 (l > 2σ (l))
Absorption correction	Semi-empirical from equivalents	Semi-empirical from equivalents	Semi-empirical from equivalents
Max. and min. transmission	0.96 and 0.84	0.75 and 0.70	0.77 and 0.70
Refinement method	Full-matrix least-squares on F^2	Full-matrix least-squares on F^2	Full-matrix least-squares on F^2

Data/restraints/parameters	2752 / 0 / 217	8497 / 0 / 325	8898 / 0 / 379
Goodness-of-fit on F^2	1.01	1.03	1.02
Final R indices (l>2sigma(l))	R1 = 0.071, wR2 = 0.124	R1 = 0.025, wR2 = 0.051	R1 = 0.023, wR2 = 0.048
Absolute structure parameter	-0.4(2)	_	
Largest diff. peak and hole	0.33 and -0.29 eÅ^{-3}	0.73 and -0.65 eÅ^{-3}	0.88 and -0.87 eÅ^{-3}

Table S2. Selected bond angles and distances of **1** and **2**, before and after forming the co-assembly with TFDIB.

	Compound 1	**Compound 2**
π-π in the co-assembly (Å)	3.348 (3)	3.478 (4)
P-O distance (Å)	1.484 (5)	1.491 (4)
P-O distance in the co-assembly (Å)	1.4906 (16)	1.491 (2)
P-O angle (°)	124.2 (3)	124.73 (3)
P-O angle in the co-assembly (°)	117.29 (7)	126.38 (8)
(P)O···I distance (Å)	2.786 (2)	2.816 (2)
N···I distance (Å)	2.947 (2)	2.849 (2)
(P)O···I-C angle (°)	128.95 (8)	174.7 (1)
N···I-C angle (°)	162.16 (8)	178.63 (9)
C-I(O) distance in the TFDIB after co-assembly (Å)	2.096 (2)	2.093 (3)
C-I(N) distance in the TFDIB after co-assembly (Å)	2.092 (2)	2.103 (2)

2.3. DFT Calculations

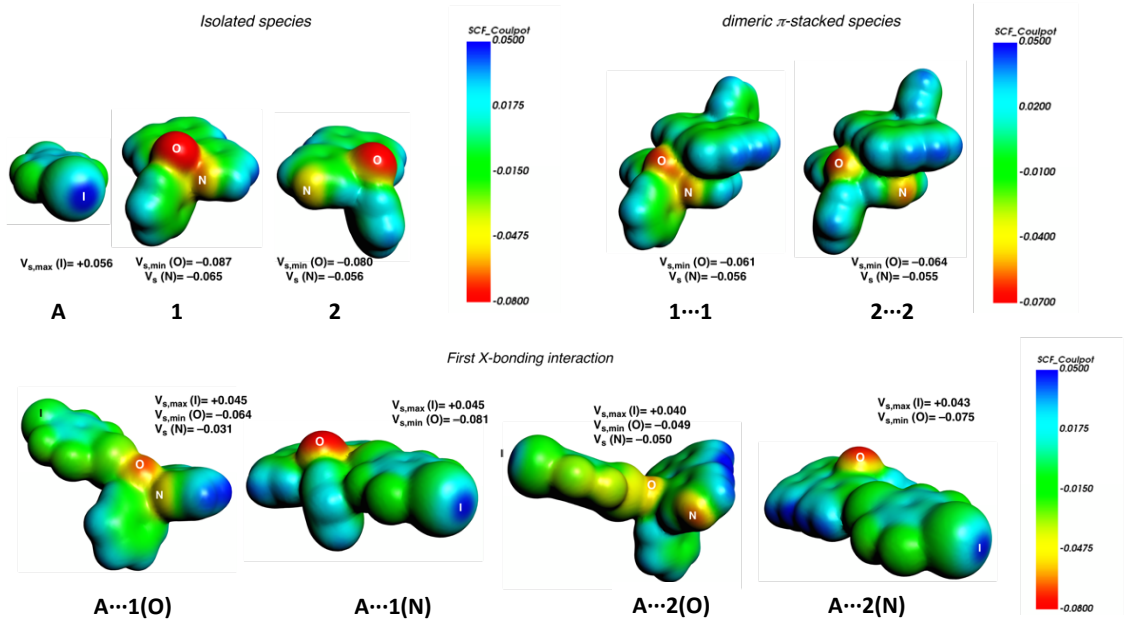

Figure S6. Electrostatic surface potentials (ESP) mapped on the 0.001 a.u. electron isodensity and the estimated maximum and minimal values ($V_{s,max}$ and $V_{s,min}$) at the O as well as at the N atom computed at wBP97-XD/TZVP level. Color scale and V_s values are in a.u.

Table S3. EDA of the interaction energy of I–bonded complexes computed at wB97–XD/TZVP level in kcal mol^{-1}. See equation (1) for further definition of each term.

entry	Interaction	ΔV_{elstat}	ΔE_{Pauli}	ΔE_{oi}	ΔE_{disp}	ΔE_{int}
1	**1**(PO)···**A**	-15.09	12.94	-7.49	-3.49	**-13.12**
2	**1**(N)···**A**	-14.57	13.06	-6.28	-5.03	**-12.82**
3	**2**(PO)···**A**	-11.22	8.96	-5.47	-1.96	**-9.69**
4	**2**(N)···**A**	-16.84	16.97	-7.29	-2.10	**-9.27**
5	**1**(PO)-**A**···(OP)**1**	-14.45	13.11	-7.12	-3.50	**-11.97**
6	**1**(PO)-**A**···(N)**1**	-14.57	13.05	-7.23	-3.52	**-12.26**
7	**1**(N)-**A**···(OP)**1**	-13.04	13.45	-6.02	-5.07	**-10.69**
8	**1**(N)-**A**···(N)**1**	-14.32	13.16	-6.16	-5.06	**-12.37**
9	**2**(PO)-**A**···(OP)**2**	-10.15	9.08	-5.17	-1.97	**-8.21**
10	**2**(PO)-**A**···(N)**2**	-15.33	15.86	-6.45	-2.09	**-8.01**
11	**2**(N)-**A**···(OP)**2**	-10.42	9.06	-5.24	-1.97	**-8.57**
12	**2**(N)-**A**···(N)**2**	-16.38	17.09	-6.99	-2.11	**-8.39**

Table S4. EDA of the interaction energy for the formation of the dimers and X–bonded complexes considering dimers computed at the wB97–XD/TZVP level of theory. All contributions are in kcal mol^{-1}.

entry	Interaction	ΔV_{elstat}	ΔE_{Pauli}	ΔE_{oi}	ΔE_{disp}	ΔE_{int}
1	**1**···**1**	–18.14	6.06	–7.65	–15.40	**–35.13**
2	**2**···**2**	–13.34	2.76	–5.41	–15.36	**–31.34**
3	Dim^1(PO)···**A**	–15.82	13.27	–7.30	–4.94	**–14.79**
4	Dim^1(N)···**A**	–15.82	13.48	–6.78	–6.19	**–15.30**
5	Dim^2(PO)···**A**	–12.67	9.81	–5.79	–4.02	**–12.67**
6	Dim^2(N)···**A**	–18.47	17.47	–8.20	–3.92	**–13.12**
7	Dim^1(PO)-**A**···(OP)Dim^1	–16.02	13.39	–7.08	–4.99	**–14.70**
8	Dim^1(PO)-**A**···(N)Dim^1	–14.04	13.63	–6.52	–6.11	**–13.04**
9	Dim^1(N)-**A**···(OP)Dim^1	–15.54	13.38	–7.12	–5.02	**–14.30**
10	Dim^1(N)-**A**···(N)Dim^1	–15.88	13.58	–6.60	–6.26	**–15.16**
11	Dim^2(PO)-**A**···(OP)Dim^2	–12.34	9.90	–5.63	–4.06	**–12.13**
12	Dim^2(PO)-**A**···(N)Dim^2	–17.24	16.38	–7.51	–3.99	**–12.37**
13	Dim^2(N)-**A**···(OP)Dim^2	–12.07	9.92	–5.64	–4.07	**–11.86**
14	Dim^2(N)-**A**···(N)Dim^2	–18.20	17.58	–7.95	–3.96	**–12.52**

Within the EDA framework, the interaction energy is decomposed as: a) electrostatic interaction ($\Delta V_{elstat}(\zeta)$): it represents the classical Coulombic interaction between the unperturbed charge distribution of each of the two fragments; b) Pauli repulsions ($\Delta E_{Pauli}(\zeta)$) between occupied orbitals of the two fragments: it is responsible for steric repulsion; c) $\Delta E_{oi}(\zeta)$ stands for the stabilizing orbital interaction energy including charge transfer; d) dispersion energy (ΔE_{disp}): it corresponds to the dispersion interactions

2.4. Spectroscopic data

Table S5. Summary of the photophysical properties of **1** and **2**.[S1c]

	Compound 1	**Compound 2**
Φ[a]	0.12	0.14
τ (ns)[b]	0.87	0.9
Absorp. λ_{max} (nm)[d]	334, 349	336, 351
Emission λ_{max} (nm)[e]	364(sh), 381	367(sh), 383
k_r (10^8 s^{-1})	1.38	1.56
k_{nr} (10^8 s^{-1})	10.1	9.56

[a] Fluorescence quantum yields relative to quinine sulfate in 0.1 M H_2SO_4, $\Phi = 0.54$. [b] Fluorescence lifetimes. [c] Molar extinction coefficient of the absorption maxima. [d] Absorption maxima recorded from CH_2Cl_2 solutions. [e] Emission maxima recorded from CH_2Cl_2 solutions. (sh) = shoulder.

2.5. NMR data

^{1}H NMR (600 MHz, $CDCl_3$) of 1

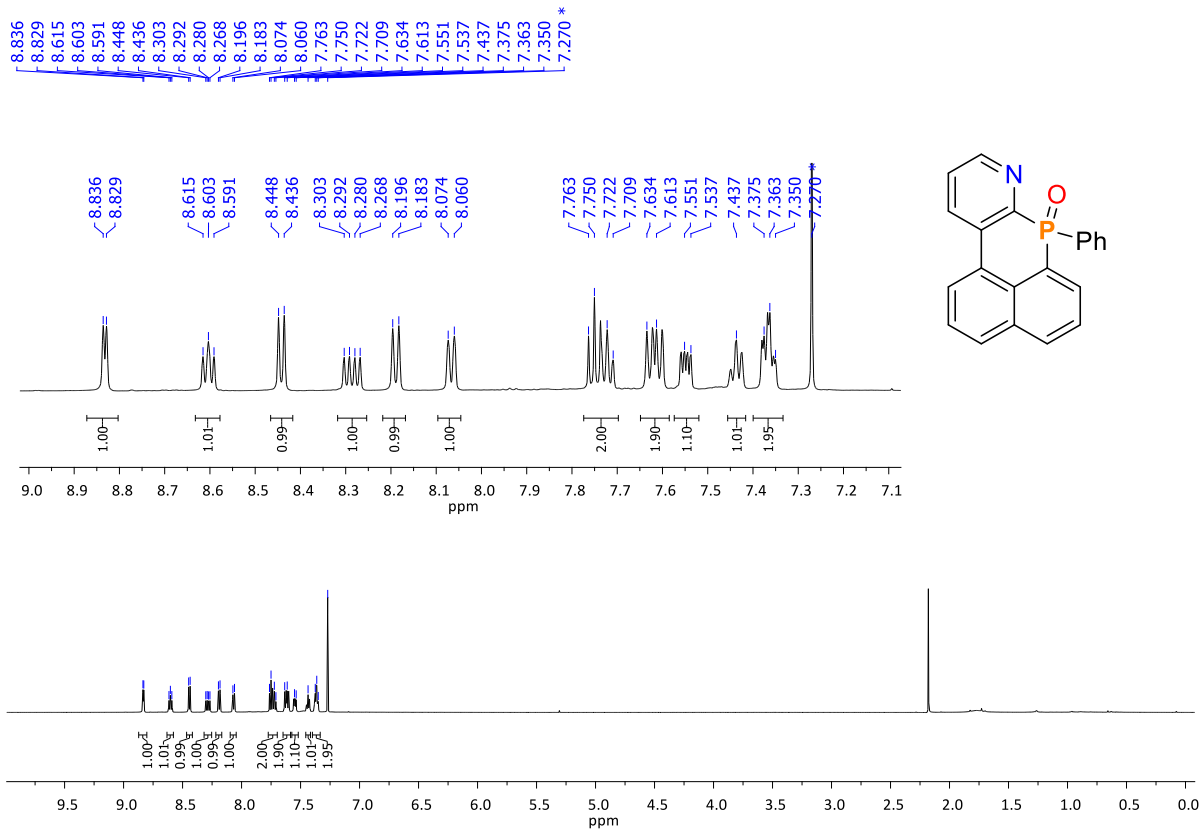

^{1}H-^{1}H COSY NMR (400 MHz, $CDCl_3$) of 1

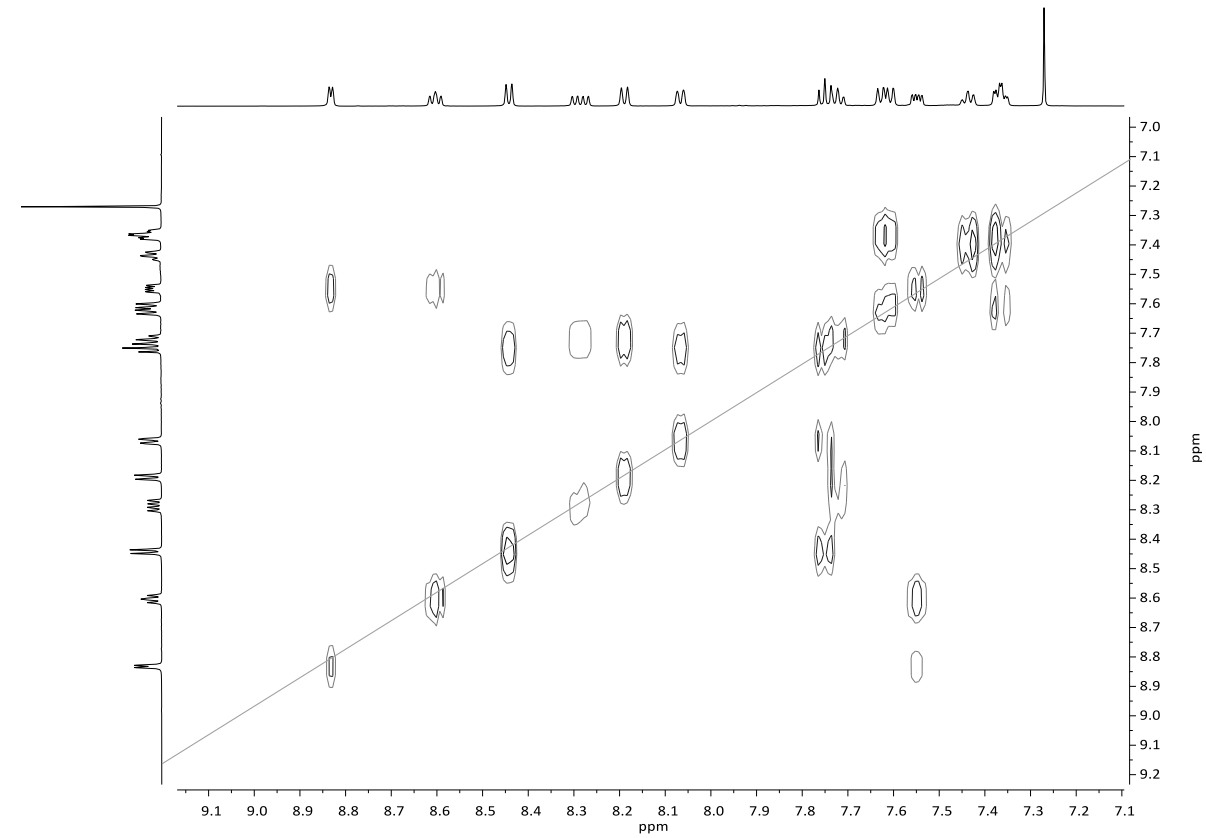

$^{13}C\{1H\}$ NMR (151 MHz, $CDCl_3$) of 1

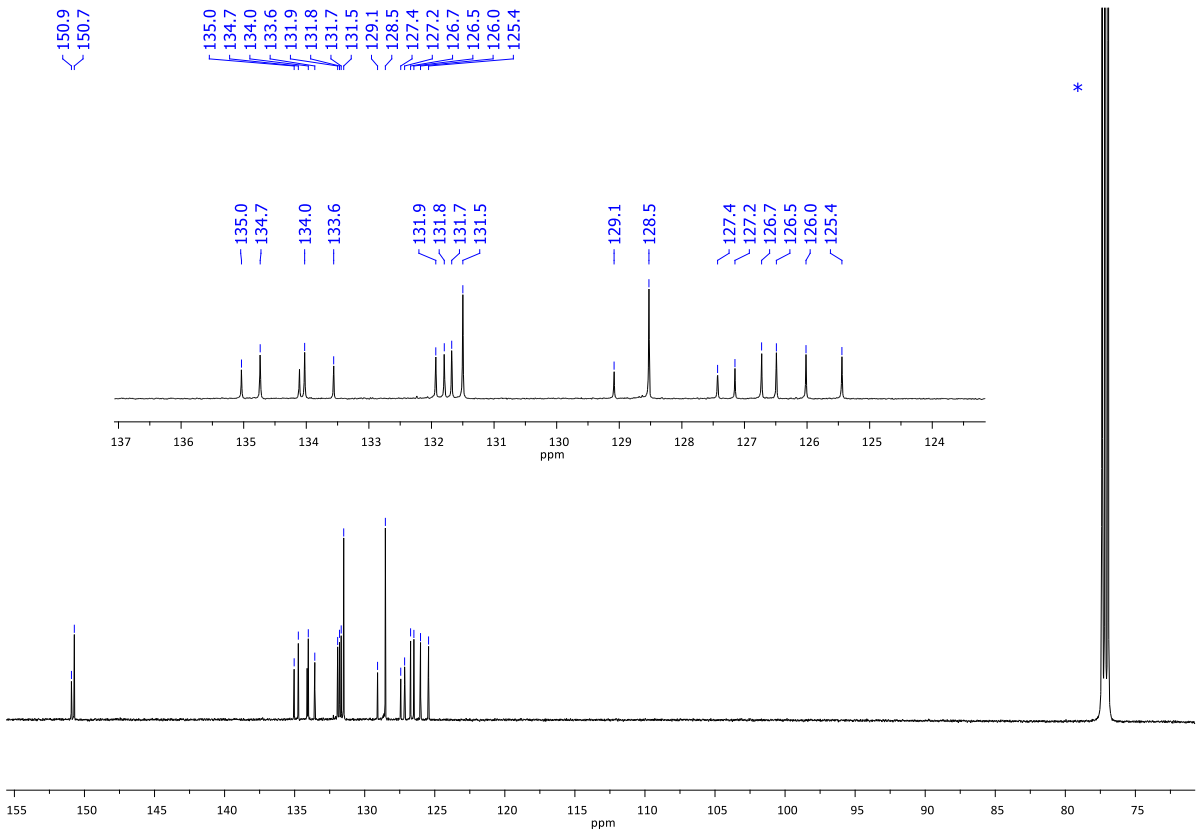

$^{31}P\{1H\}$ NMR (243 MHz, $CDCl_3$) of 1

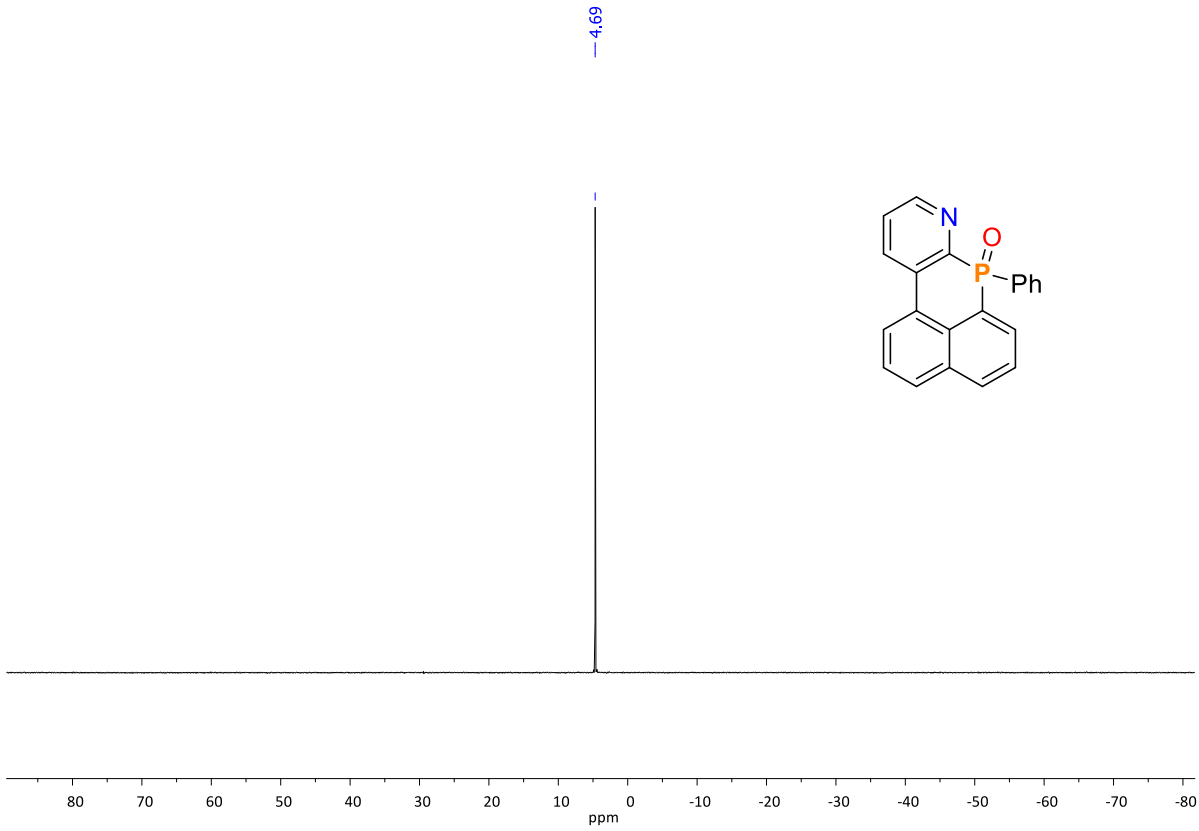

3. Literature

S1. a) A. Bouillon, J.-C. Lancelot, V. Collot, P.R. Bovy and S. Rault, *Tetrahedron*, 2002, **58**, 3323–3328; b) H.-Q. Do and O. Daugulis, *Org. Lett.*, 2009, **11**, 421–423; c) C. Romero-Nieto, A. López-Andarias, C. Egler-Lucas, F. Gebert, J.-P. Neus and O. Pilgram, *Angew. Chem. Int. Ed.*, 2015, **54**, 15872–15875; *Angew. Chem.*, 2015, **127**, 16098–16102.

S2. Program SADABS 2008/1 for absorption correction; G. M. Sheldrick, Bruker Analytical X-ray-Division, Madison, Wisconsin 2012.

S3. Software package SHELXTL 2008/4 for structure solution and refinement; G.M. Sheldrick, *Acta Cryst.* 2008, **A64**, 112–122.

S4. S.C.M. ADF2019.302 Theoretical Chemistry, Vrije Universiteit: Amsterdam, **2019**. See: www.scm.com.

S5. N. Mardirossian and M. Head-Gordon, *Phys. Chem. Chem. Phys.*, 2014, **16**, 9904–9924.

S6. (a) A. D. Becke, *Phys. Rev. A*, 1988, **38**, 3098–3100. (b) J. P. Perdew, *Phys. Rev. B*, 1986, **33**, 8822–8824.

S7. S. Grimme, J. Antony, S. Ehrlich and H. J. Krieg, *Chem. Phys.*, 2010, **132**, 154104.

S8. (a) A. Forni, S. Pieraccini, S. Rendine and M. Sironi, *J. Comput. Chem.*, 2014, **35**, 386–394. (b) L. N. Anderson, F. W. Aquino, A. E. Raeber, X. Chen and B. M. Wong, *J. Chem. Theory Comput.*, 2018, **14**, 180–190.

S9. E. van Lenthe, E. J. Baerends and J. G. Snijders, *J. Chem. Phys.*, 1994, **101**, 9783–9792.

S10. a) F. M. Bickelhaupt and E. J. Baerends, in *Reviews in Computational Chemistry*, ed. K. B. Lipkowitz and D. B. Boyd, Wiley–VHC, New York, 2000, pp. 1–86. (b) M. Lein and G. Frenking, in *Theory and Applications of Computational Chemistry. The First Forty Years*, ed. C. E. Dykstra, G. Frenking, K. S. Kim, G. E. Scuseria, Elsevier, Amsterdam, 2005, pp. 291–372.

S11. C. Fonseca Guerra, J. W. Handgraaf, E. J. Baerends and F. M Bickelhaupt, *J. Comput. Chem.*, 2004, **25**, 189–210.

S12. W. H. Melhuish, *J. Phys. Chem.*, 1961, **65**, 229–235.